

Broddingnagian photon bunching in cathodoluminescence of excitons in WS₂ monolayer

Saskia Fiedler,^{1,*} Sergii Morozov,^{1,2,*} Leonid Iliushyn,^{2,3} Sergejs Boroviks,¹ Martin Thomaschewski,¹ Jianfang Wang,⁴ Timothy J. Booth,^{2,3} Nicolas Stenger,^{2,5} Christian Wolff,¹ and N. Asger Mortensen^{1,2,6,†}

¹Center for Nano Optics, University of Southern Denmark, Campusvej 55, DK-5230 Odense M, Denmark

²Center for Nanostructured Graphene, Technical University of Denmark, DK-2800 Kongens Lyngby, Denmark

³Department of Physics, Technical University of Denmark, DK-2800 Kongens Lyngby, Denmark

⁴Department of Physics, The Chinese University of Hong Kong, Shatin, Hong Kong SAR, China

⁵Department of Photonics Engineering, Technical University of Denmark, DK-2800 Kongens Lyngby, Denmark

⁶Danish Institute for Advanced Study, University of Southern Denmark, Campusvej 55, DK-5230 Odense M, Denmark

ABSTRACT Cathodoluminescence spectroscopy in conjunction with second-order auto-correlation measurements of $g_2(\tau)$ allows to extensively study the synchronization of quantum light sources in low-dimensional structures. Co-existing excitons in two-dimensional transition metal dichalcogenide monolayers provide a great source of identical quantum emitters which can be simultaneously excited by an electron. Here, we demonstrate large photon bunching with $g_2(0)$ up to 156 ± 16 of a tungsten disulfide monolayer (WS₂), exhibiting a strong dependence on the electron-beam current density. To further improve the excitation synchronization and the electron-emitter interaction, we show exemplarily that the careful selection of a simple and compact geometry – a thin, monocrystalline gold nanodisk – can be used to realize a record-high bunching $g_2(0)$ of up to 2152 ± 236 . This approach to control the electron excitation of excitons in a WS₂ monolayer allows for the synchronization of quantum emitters in an ensemble, which is important to further advance quantum information processing and computing technologies.

Keywords: Broddingnagian photon bunching, cathodoluminescence, transition metal dichalcogenide monolayer, hexagonal boron nitride, monocrystalline gold nanodisk.

INTRODUCTION

The recent development in the synthesis and the fabrication of two-dimensional (2D) transition metal dichalcogenide (TMDC) monolayers has sparked intensive research of their implementation in applications in the emerging field of quantum information and computing technologies [1, 2]. The family of TMDC monolayers with a thickness of a few atoms provides an attractive combination of optoelectronic properties, including a direct bandgap, a strong spin-orbit coupling and splitting, an access to spin and valley degrees of freedom [3]. An isolated monolayer is a robust material platform for quantum light generation, where the co-existence of multiple excitons is a resource that represents an ensemble of identical quantum light sources.

Photon statistics and second-order auto-correlation function $g_2(\tau)$ constitute powerful indicators for the identification of single-photon sources in various solid-state platforms, while also giving insight into the quantum-mechanical correlation between emitters within an ensemble. The spontaneous emission of an individual quantum emitter results in a stream of single photons which exhibits the characteristic dip at zero delay time in the photon-correlation histogram (photon anti-bunching). In contrast, photon statistics of an ensemble formed by identical quantum emitters, localized within a sub-wavelength volume, strongly depends on the excitation synchronization and can exhibit cooperative spontaneous emission (photon bunching) [4].

Photoexcitation of quantum ensembles does not provide the required synchronization as the photon arrival statistics is Poissonian in nature. Therefore, a large ensemble typically exhibits a flat second-order auto-correlation function $g_2(\tau) \rightarrow 1$. To

break the $g_2(\tau = 0) = 1$ limit, a high synchronization of emitters is required, and such an ensemble exhibits a peak at zero correlation time, that is $g_2(0) > 1$. This can be achieved by emitter entanglement through a shared electromagnetic mode [5–7]. The width of the bunching peak provides information about the emission lifetime of the emitters, while its amplitude indicates the probability of the excitation to interact with an emitter [8].

Photon bunching has been observed using low-current electron-beam excitation, namely cathodoluminescence (CL) [9]. In the limit of high electron-beam current, the electron arrival approaches Poissonian statistics, thus resulting in a flat second-order auto-correlation function $g_2(\tau) \rightarrow 1$ as in the case of photoexcitation. However, reducing the electron-beam current to sub-few hundred pA breaks the Poissonian statistics and an arriving electron will potentially generate multiple iden-

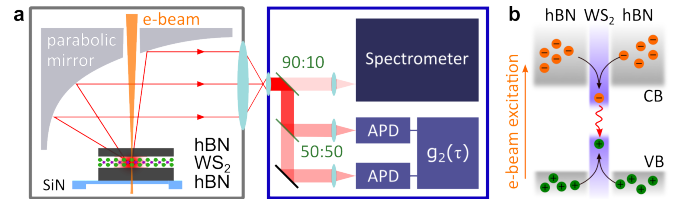


Figure 1: Electron-beam excitation of hBN-encapsulated WS₂ monolayer. **a** Schematics of the experimental setup for detection of electron-beam-induced emission from a WS₂ monolayer. The generated emission is collected with a parabolic mirror and directed towards a spectrometer and HBT interferometer consisting of two avalanche photodiodes (APD) and a 50:50 beamsplitter. **b** Electron beam generates electron-hole pairs in hBN, which relax to WS₂ conduction and valence bands (CB and VB) with subsequent synchronized radiative recombination.

tical electron-hole pairs capable of synchronized excitation of a quantum ensemble. The synchronized radiative recombination does not necessarily imply phase locking, thus can be considered as simultaneous emission of emitters in an ensemble triggered by the same electron. Exploiting the low currents, quantum ensembles in various solid state systems – such as indium gallium nitride (InGaN) quantum wells and color centers in nano-diamonds – have been shown to generate quantum light with $g_2(0)$ up to 80 [10, 11]. A decrease of the electron-beam current to sub-pA is expected to further increase the $g_2(0)$ -values, however such low currents are unattainable by state-of-the-art instrumentation scanning electron microscopes (SEMs). While in transmission electron microscopes (TEMs) the electron-beam current can be readily further reduced, the substantially smaller spot size results in an increased current density, which we will demonstrate in the following to be one of the key controls over the bunching factor. Therefore, to further boost the photon bunching, two requirements need to be met, (i) quantum ensembles consisting of identical and densely localized emitters within a sub-wavelength volume, and (ii) a geometry increasing the probability of electron-emitter interaction.

In this letter, we study the luminescence properties and photon statistics of a tungsten disulfide (WS_2) monolayer encapsulated in hexagonal boron nitride (hBN) layers. We report the first observation of photon bunching in a WS_2 monolayer under electron-beam excitation, which reaches $g_2(0) = 156 \pm 16$ at the lowest attainable current by our instrument. We further explore methods for improving the excitation synchronization and electron-emitter interaction via adding a monocrystalline gold nanodisk. In such a geometry, we achieve record-high photon bunching of $g_2(0) = 2152 \pm 236$, exceeding the previously reported values by over an order of magnitude. Our simple geometry offers a robust and compact platform to generate quantum light with Brodbingnagian [12] photon bunching statistics, which has important applications in quantum information processing and computing technologies.

RESULTS AND DISCUSSION

Sample and experimental setup

We perform photoluminescence (PL) and cathodoluminescence (CL) experiments of a WS_2 monolayer sandwiched between two thin hBN flakes (see SI Fig. S1). The hBN encapsulation on both sides of the WS_2 monolayer serves three purposes: (i) protecting the WS_2 from electron-beam damage and contamination, (ii) increasing the effective interaction volume of incoming electrons with the monolayer, and (iii) providing layers for the generation of additional charge carriers which can subsequently diffuse into the WS_2 and radiatively recombine, thereby significantly enhancing the CL intensity [13]. We note that even smallest contamination during the assembly of hBN- WS_2 -hBN heterostructure can cause quick and irreversible degradation of the WS_2 monolayer under the electron

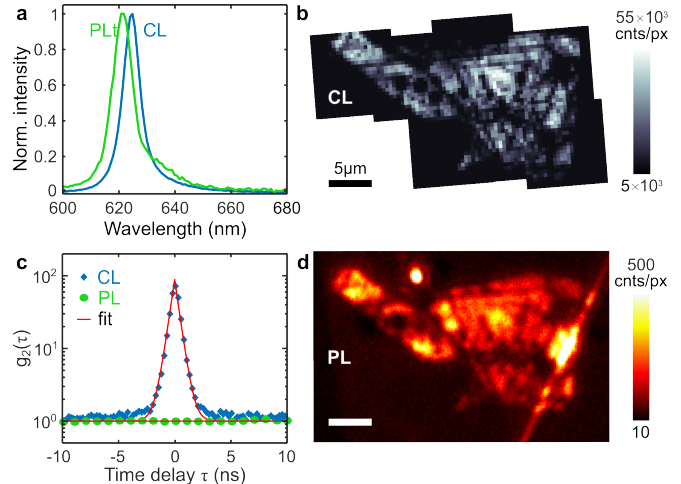


Figure 2: Photo- and electron-beam excitation of hBN-encapsulated WS_2 monolayer. **a** PL and CL spectra of WS_2 -hBN heterostructure. **b** CL intensity map obtained by electron-beam scanning of the sample. **c** Electron-beam excitation synchronizes emitters, leading to the photon bunching, while photoexcitation only generates a flat $g_2(0) = 1$. **d** PL intensity map of the sample obtained by confocal scanning.

beam. Fig. 1a schematically presents the experimental setup for the electron-beam excitation of the hBN- WS_2 -hBN sample and the collection of the generated CL. Here, the electron beam is focused onto the hBN- WS_2 -hBN stack, and the generated CL is subsequently collimated by a parabolic mirror and focused onto a spectrometer and a Hanbury Brown and Twiss (HBT) interferometer (see SI).

Photo and electron-beam excitation

Photo and electron-beam excitation are essentially different mechanisms of exciton generation in a WS_2 monolayer. An incoming photon typically creates one electron-hole pair in the WS_2 monolayer, while an incoming electron can excite many electron-hole pairs in the sample (Fig. 1b), predominantly in the thicker hBN layers due to a large interaction volume [14]. The latter process can be described by a scattered incoming electron which excites high-energy interband transitions in the sample, also referred to as bulk plasmons in electron spectroscopy literature [9, 15, 16]. Such bulk plasmons are comprised of a coherent sum of interband transitions contrary to the collective intraband oscillations of free charges, e.g., manifesting in surface plasmons. They subsequently decay into multiple identical electron-hole pairs which, after the typical excitonic lifetime, exhibit synchronized radiative recombination. The photons appear to arrive as a "packet" and can be detected with the HBT interferometer as photon bunching ($g_2(0) > 1$).

In Fig. 2a, we compare spectral emission properties of the hBN- WS_2 -hBN stack under photo- and electron-beam excitation. The PL spectrum is centered around 621 nm and has

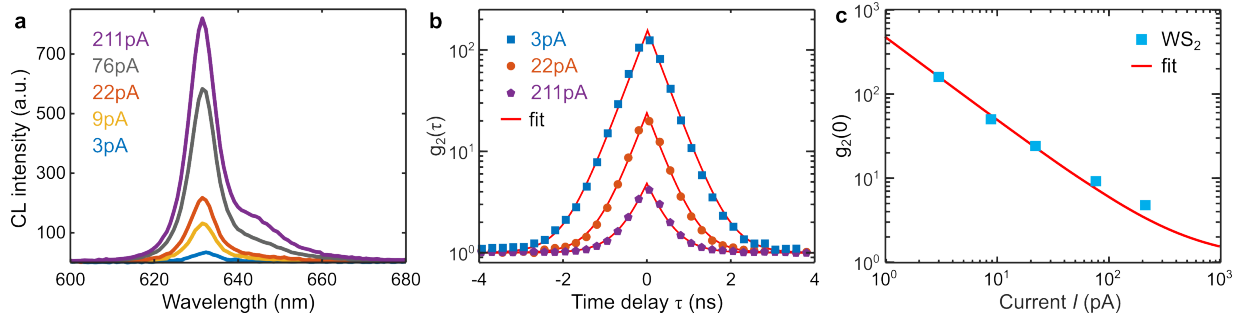


Figure 3: Cathodoluminescence of hBN-encapsulated WS₂ monolayer at low and high electron-beam current. **a** 10 kV-CL spectra demonstrate the growth of CL intensity at increasing electron-beam current. Trion emission accompanies the neutral exciton at high electron-beam currents. **b** Photon correlation histograms show reduction of photon bunching with increasing electron-beam current. **c** Photon bunching factor $g_2(0)$ exhibits inverse dependence with electron-beam current.

a red-shifted satellite peak at 635 nm (green line in Fig. 2a). These emission lines are characteristic for the neutral and red-shifted charged exciton (trion) in WS₂ monolayers at room temperature [17]. The CL spectrum in Fig. 2a is dominated by the neutral exciton peak at 626 nm which is red-shifted with respect to the PL spectrum. In general, we observe a sub-10 nm spectral wandering of the excitonic peak in both PL and CL measurements which is possibly due to local strain within the WS₂ monolayer [18]. Fig. 2b presents a CL intensity map obtained by scanning the electron beam over the hBN-WS₂-hBN sample. The spatial CL distribution reveals areas of lower intensity, which are due to cracks in the WS₂ monolayer. The round dark patches apparent in the CL map can be attributed to bubbles in between the three layers, as the lack of adherence in the stacked sample has been shown to result in quenched luminescence [19]. Fig. 2d displays a corresponding PL confocal map obtained with laser excitation at 404 nm. We find a similar intensity distribution as in the CL map in Fig. 2b, although characterized by a lower spatial resolution than with an electron beam.

The photon statistics of emission generated from the hBN-WS₂-hBN sample drastically depend on the type of excitation. Fig. 2c presents photon correlation histograms obtained under photo and electron-beam excitation. Electron-beam excitation results in a pronounced photon bunching peak at zero correlation time (blue diamonds in Fig. 2c), while the photon correlation histogram obtained under photoexcitation is flat with $g_2(0) = 1$ (green circles in Fig. 2c). Moreover, the bunching amplitude in CL can be tuned by the electron-beam current (which we demonstrate in the next section), unlike the flat photon correlation histogram in PL [9].

CL response to electron-beam current

The CL intensity and the amplitude of photon bunching can be controlled by the electron-beam current I . As the electron-beam current is increased, a higher CL intensity is observed due to the larger amount of incoming electrons, generating more electron-hole pairs in the sample, which can subsequently

recombine radiatively in the WS₂ monolayer (Fig. 3a). In contrast, the amplitude of the photon bunching peak follows the opposite trend: with increasing I , the contribution of uncorrelated emission is increased, resulting in a lower photon bunching (see SI Fig. S2). Fig. 3b shows the bunching histograms collected at low and high electron-beam currents, which we fit to extract the values of $g_2(0)$ (see SI). At the lowest electron-beam current of 3 pA, we achieve a giant bunching factor 156 ± 16 , indicating the high quality of the investigated sample. In contrast, the bunching factor is greatly reduced to approximately 4.7 ± 0.2 for the highest electron-beam current of 211 pA. The I -dependent photon bunching factors are summarized in Fig. 3c. We fit the examined dynamics with $g_2(0, I) = 1 - I_0/I$ as the bunching factor has been observed to be inversely dependent on the applied electron-beam current [9, 16]. Here, I_0 is a free parameter describing the probability of the electron beam interacting with the emitters.

The mechanism behind the photon bunching can be attributed to the synchronization of emission from emitters, where each incoming electron creates a photon packet. With increasing electron-beam current, the electrons arrive closer in time and the photon packets become increasingly indistinguishable, thereby reducing the bunching factor until the Poissonian distribution $g_2(0, I \rightarrow \infty) = 1$ is reached. In the hBN-WS₂-hBN-sample, the inverse I -dependence is confirmed in Fig. 3c, although the Poissonian distribution cannot be reached due to sample degradation at high electron-beam currents $I > 250$ pA (see SI Fig. S3).

Boosting bunching through geometry

A further increase of the photon bunching factor by reducing the applied electron-beam current is limited by the instrument. Decreasing the acceleration voltage potentially allows to reduce the current to sub-pA, however in practice, it causes severe sample charging already at 5 kV. To overcome this limit, we suggest to modify the geometry by adding a thin gold nanodisk to induce a local change of electron-beam excitation parameters. We drop-cast monocrystalline gold nanodisks with

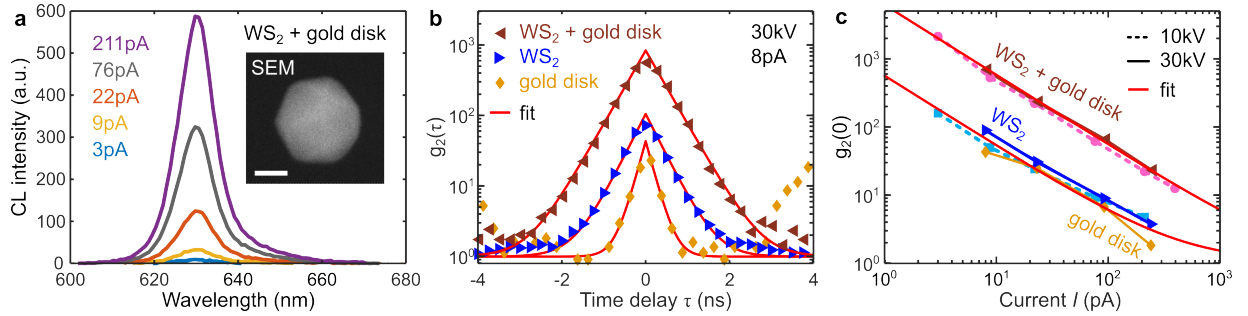


Figure 4: Enhancing electron beam interaction with the sample using a gold nanodisk. **a** 10 kV-CL spectra of hBN-encapsulated WS₂ monolayer excited through a gold nanodisk with a diameter of 120 nm using electron-beam currents ranging from 3 pA to 211 pA. The inset shows an SEM image of the gold nanodisk. The scale bar denotes 50 nm. **b** Photon correlation histograms of hBN-encapsulated WS₂ monolayer (blue triangles), hBN-encapsulated WS₂ monolayer with an Au nanodisk on top (dark red triangles), and a similar 120 nm-sized Au nanodisk on hBN (orange diamonds). **c** Photon bunching factor $g_2(0)$ vs. electron-beam current I at 10 kV (dashed lines) and 30 kV (solid lines) for the three samples as in **b**.

a diameter ranging from 80 nm to 230 nm on top of the hBN-WS₂-hBN-stack (see SEM image in SI Fig. S1). For further CL studies, we chose an Au nanodisk with an approximate diameter of 120 nm, as shown in the inset of Fig. 4a. The reasoning behind this selection is that the (broad) plasmonic dipole mode spectrally overlaps with the WS₂-exciton, in principle allowing for plasmonic interaction [20]. Fig. 4a presents the CL spectra of the hBN-WS₂-hBN-stack excited through the 120 nm-Au nanodisk with increasing electron-beam current. We observe an overall CL brightening with increasing I , similar to the bare hBN-WS₂-hBN-sample. However, the CL spectra do not reveal any emission enhancement which would indicate a plasmon-assisted Purcell effect, nor any evidence of strong coupling (Fig. 4a). This observation is in agreement with the PL measurements, where the position of the Au nanodisks distributed over the entire hBN-WS₂-hBN-sample cannot be made out. We ascribe this lack of luminescence enhancement to the large separation of 35 nm between the gold nanodisk and the WS₂ monolayer, which does not allow for efficient near-field interaction.

Remarkably, the addition of Au nanodisks improves the emission synchronization in the WS₂, and drastically affects the photon bunching factor. The Au nanodisks themselves – on hBN only – exhibit dim CL emission (see SI Fig. S3-S4), which allowed us to quantify the bunching factor to $g_2(0) = 43.1 \pm 4.9$ of a similarly sized 120 nm nanodisk (orange in Fig. 4b). Fig. 4b further compares the photon correlation histograms measured at identical excitation parameters (8 pA, 30 kV) from the hBN-WS₂-hBN stack (blue), and a system of a 120 nm-Au nanodisk on hBN-WS₂-hBN-stack (dark red). The fit of the histograms provides information about the lifetime of the generated emission τ and the bunching factor $g_2(0)$. We observe a minor change in emission lifetime of WS₂ after the addition of the Au nanodisk, extracting values of $\tau_{\text{WS}_2} = 365 \pm 18$ ps and $\tau_{\text{WS}_2+\text{Au}} = 416 \pm 10$ ps. The extracted values of exciton lifetime are in a good agreement with one obtained via time-correlated single-photon counting (TCSPC) methods using a pulsed laser ($\tau_{\text{WS}_2}^{\text{PL}} = 296 \pm 22$ ps, see SI Fig.S9). Therefore,

we conclude that the addition of an Au nanodisk did not facilitate the creation of additional, faster relaxation channels for the WS₂-excitons which is in agreement with the absence of Purcell enhancement. For the bare Au nanodisk, however, we measure a lifetime of $\tau_{\text{Au}} = 196 \pm 34$ ps, which is close to the temporal limit of our setup (180 ps). We also extract a photon bunching factor of 105 ± 11 for the bare hBN-WS₂-hBN-sample, which greatly increases to 829 ± 114 for the system of the 120 nm-Au nanodisk on the hBN-WS₂-hBN-stack at 30 kV. A simple addition of the bunching factors of the bare Au nanodisk and that of the hBN-encapsulated WS₂ cannot explain the huge increase of bunching to 829 ± 114 (which we will focus on in the next section). The highest bunching factor of 2152 ± 236 , we observe at the lowest electron-beam current of 3 pA (at 10 kV) for the Au nanodisk on the hBN-WS₂-hBN-sample (pink circles in Fig. 3c).

Finally, we confirm the inverse electron-beam current dependence of the photon bunching using a different geometry and a reduced acceleration voltage (from 30 kV to 10 kV allowing for a further reduction in I). We plot the summary of the results in Fig. 4c, including fits of the $g_2(0, I)$ -data with an inverse current function (red curves). We extract from the fit a large change in I_0 from $I_0^{\text{WS}_2} = 477 \pm 14$ pA to $I_0^{\text{WS}_2+\text{Au}} = 5257 \pm 154$ pA, which indicates the change of probability of electrons to interact with the sample due to the presence of an Au nanodisk.

Simulations of electron trajectories

We perform Monte Carlo simulations [21] to shed light on the large bunching enhancement of the hBN-WS₂-hBN-sample caused by the addition of an Au nanodisk. Fig. 5a,b present the results for electron trajectory simulations of the investigated geometries using a 10 kV-electron beam with a spot size of 5 nm. Here, the blue lines represent the primary electrons within the sample stack, while the red ones denote the back-scattered electrons (BSE). At the position of the WS₂ monolayer, marked as a thin green line in Fig. 5c, the spatial

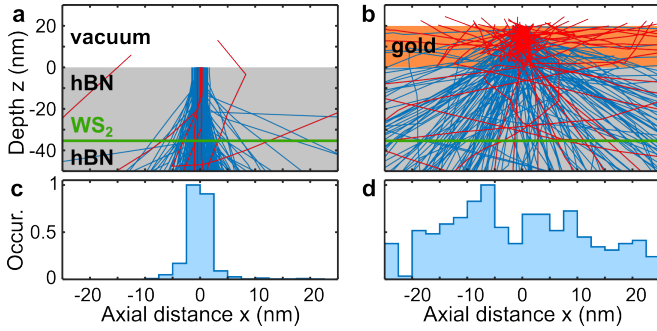


Figure 5: Diverging electron trajectories. **a** Monte Carlo simulation of 10 kV-electron-beam exposure of bare hBN-WS₂-hBN. The position of WS₂ is highlighted by a horizontal green line. Blue and red traces represent primary and back-scattered electrons, respectively. **b** Same simulation as in **a** with a 20 nm Au disk on top of the hBN-WS₂-hBN heterostructure. **c-d** Divergence of electron trajectories at the position of WS₂ monolayer for the geometries presented in panels **a-b**.

distribution of the primary electrons remains close to the original 5 nm-electron-beam diameter. In the case of an additional 20 nm-thin gold film on the topmost layer (cf. Fig. 5b), representing the Au nanodisk, the primary electrons are widely scattered within the sample resulting in enormous spread of the electron beam. In fact, the divergence is so large that no clear electron-beam diameter can be assigned within the range of 50 nm which is depicted in Fig. 5d. This huge spread of the electron beam reduces the effective electron density at the position of the WS₂ monolayer which is equivalent to a reduced current at a given sample area. As a result, the photon bunching is greatly increased.

We conclude that the electron current density ultimately determines the photon bunching in CL; not only the temporal distance between electrons plays a crucial role but also spatial distance. This implies that within the lifetime of the exciton there is no other electron passing by within the correlation length of the electronic system. Otherwise, it would add Poissonian noise and thereby limit the $g_2(0)$. To verify experimentally this important finding, we mimic the spread of the electron beam at the position of the WS₂ monolayer by manually defocusing the electron beam. Here, we increase the working distance which effectively spreads the electron beam to larger spot sizes without changing the initial electron-beam parameters, such as acceleration voltage and current. We observe a similar trend of high photon bunching factors with increasing defocus, while we do not record any substantial change in CL intensity (see SI Fig. S5). Although this effect of widely spread electrons is by far less pronounced than that of an additional thin Au nanodisk, the trend clearly indicates that the effective electron density at the position of the monolayer governs the resulting photon bunching.

CONCLUSION AND OUTLOOK

In conclusion, we demonstrated the importance of electron-beam excitation for synchronization of large emitter ensembles, and for achieving high photon bunching factors. We reported a high photon bunching in cathodoluminescence ($g_2(0) = 156 \pm 16$) in a WS₂ monolayer encapsulated in hBN. We further suggested that an appropriate geometry can locally modify the electron-beam interaction with the sample, which allows to boost the photon bunching dynamics far beyond the instrumentation-limited currents. We utilized a system of a 20 nm-thin gold nanodisk on a hBN-WS₂-hBN-stack to demonstrate Brodbingnagian photon bunching of $g_2(0) = 2152 \pm 236$, which is over an order of magnitude larger than previously reported values. Employing Monte Carlo simulations in combination with CL- $g_2(\tau)$ -measurements, we showed that the effective electron current density at the position of the WS₂ monolayer essentially determines the resulting photon bunching factor. We presented a simple way to drive the values of $g_2(0)$ to extremes, which offers a novel source with Brodbingnagian photon bunching for applications in quantum computing and information technologies.

SUPPORTING INFORMATION

The Supporting Information includes details on sample fabrication; cathodoluminescence spectroscopy; photon correlation measurements; imaging of hBN-encapsulated WS₂ monolayer; uncorrelated emission contribution at high electron-beam currents; analysis of CL intensity at low and high electron-beam currents; CL spectrum of a gold nanodisk; effect of electron-beam defocusing on photon correlation; background emission from the substrate; Raman characterization of the sample; lifetime measurements.

ACKNOWLEDGMENTS

The authors gratefully acknowledge the experimental support of V. Zenin. N. A. M. is a VILLUM Investigator supported by VILLUM FONDEN (Grant No. 16498). S. M. acknowledges funding from the Marie Skłodowska-Curie Action (Grant agreement No. 101032967). C. W. acknowledges funding from a MULTIPLY fellowship under the Marie Skłodowska-Curie COFUND Action (Grant agreement No. 713694). The Center for Nanostructured Graphene is sponsored by the Danish National Research Foundation (Project No. DNR103).

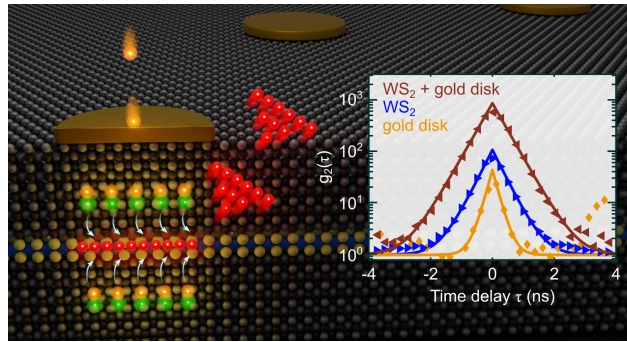
AUTHOR CONTRIBUTIONS

S. F. conceived the idea and managed the project. S. F. and S. M. designed and built the experimental setup. S. F., S. M., and M. T. performed optical measurements; S. B. and S. F. conducted Raman characterization. L. I. assembled heterostruc-

tures; J. W. synthesized monocrystalline gold nanodisks. S. F. performed the Monte Carlo simulations of electron trajectories. S. B. and S. M. prepared the cover art. S. M., S. F., and C. W. analyzed the data. The project was supervised by N. A. M., T. J. B., C. W., and N. S. The results were discussed by all authors and the writing of the manuscript was done in a joint effort. All authors provided critical feedback and helped shape the research, analysis, and manuscript.

REFERENCES

- * S. F. and S. M. contributed equally to this work.
 † asger@mailaps.org
- [1] I. Aharonovich, D. Englund, and M. Toth. Solid-state single-photon emitters. *Nat. Photon.*, 10:631–641, 2016.
 - [2] A. Reserbat-Plantey, I. Epstein, I. Torre, A. T. Costa, P. A. D. Gonçalves, N. A. Mortensen, M. Polini, J. C. W. Song, N. M. R. Peres, and F. H. L. Koppens. Quantum nanophotonics in two-dimensional materials. *ACS Photonics*, 8(1):85–101, 2021.
 - [3] S. Manzeli, D. Ovchinnikov, D. Pasquier, O. V. Yazyev, and A. Kis. 2d transition metal dichalcogenides. *Nat. Rev. Mater.*, 2(8):17033, 2017.
 - [4] V. V. Temnov and U. Woggon. Photon statistics in the cooperative spontaneous emission. *Opt. Express*, 17(7):5774–5782, 2009.
 - [5] A. Sipahigil, R. E. Evans, D. D. Sukachev, M. J. Burek, J. Borregaard, M. K. Bhaskar, C. T. Nguyen, J. L. Pacheco, H. A. Atikian, C. Meuwly, R. M. Camacho, F. Jelezko, E. Bielejec, H. Park, M. Lončar, and M. D. Lukin. An integrated diamond nanophotonics platform for quantum-optical networks. *Science*, 354(6314):847–850, 2016.
 - [6] J.-H. Kim, S. Aghaeimeibodi, C. J. K. Richardson, R. P. Leavitt, and E. Waks. Super-radiant emission from quantum dots in a nanophotonic waveguide. *Nano Lett.*, 18(8):4734–4740, 2018.
 - [7] J. Q. Grim, A. S. Bracker, M. Zalalutdinov, S. G. Carter, A. C. Kozen, M. Kim, C. S. Kim, J. T. Mlack, M. Yakes, B. Lee, and D. Gammon. Scalable in operando strain tuning in nanophotonic waveguides enabling three-quantum-dot superradiance. *Nat. Mater.*, 18(9):963–969, 2019.
 - [8] S. Meuret. Applications of photon bunching in cathodoluminescence. *Adv. Imaging Electron Phys.*, 215:47–87, 2020.
 - [9] S. Meuret, L. H. G. Tizei, T. Cazimajou, R. Bourrellier, H. C. Chang, F. Treussart, and M. Kociak. Photon bunching in cathodoluminescence. *Phys. Rev. Lett.*, 114:197401, 2015.
 - [10] S. Meuret, T. Coenen, S. Y. Woo, Y.-H. Ra, Z. Mi, and A. Polman. Nanoscale relative emission efficiency mapping using cathodoluminescence $g^{(2)}$ imaging. *Nano Lett.*, 18(4):2288–2293, 2018.
 - [11] M. A. Feldman, E. F. Dumitrescu, D. Bridges, M. F. Chisholm, R. B. Davidson, P. G. Evans, J. A. Hachtel, A. Hu, R. C. Pooser, R. F. Haglund, and B. J. Lawrie. Colossal photon bunching in quasiparticle-mediated nanodiamond cathodoluminescence. *Phys. Rev. B*, 97:081404(R), 2018.
 - [12] J. Swift. *Travels into Several Remote Nations of the World. In Four Parts. By Lemuel Gulliver, First a Surgeon, and then a Captain of Several Ships*. Benjamin Motte, London, 1726.
 - [13] S. Zheng, J.-K. So, F. Liu, Z. Liu, N. Zheludev, and H. J. Fan. Giant enhancement of cathodoluminescence of monolayer transitional metal dichalcogenides semiconductors. *Nano Lett.*, 17(10):6475–6480, 2017.
 - [14] B. G. Yacobi and D. B. Holt. *Cathodoluminescence microscopy of inorganic solids*. Springer Science+Business Media, New York, 1990.
 - [15] R. F. Egerton. *Electron energy-loss spectroscopy in the electron microscope*. Springer, New York, 2011.
 - [16] S. Meuret. *Intensity interferometry experiment: photon bunching in cathodoluminescence*, volume 215 of *Advances in Imaging and Electron Physics*. Elsevier, 2020.
 - [17] S. Morozov, C. Wolff, and N. A. Mortensen. Room-temperature low-voltage control of excitonic emission in transition metal dichalcogenide monolayers. *Adv. Opt. Mat.*, 9:2101305, 2021.
 - [18] Z. Li, Y. Lv, L. Ren, J. Li, L. Kong, Y. Zeng, Q. Tao, R. Wu, H. Ma, B. Zhao, D. Wang, W. Dang, K. Chen, L. Liao, X. Duan, X. Duan, and Y. Liu. Efficient strain modulation of 2D materials via polymer encapsulation. *Nat. Commun.*, 11(1):1151, 2020.
 - [19] G. Nayak, S. Lisi, W. L. Liu, T. Jakubczyk, P. Stepanov, F. Donatini, K. Watanabe, T. Taniguchi, A. Bid, J. Kasprzak, M. Richard, V. Bouchiat, J. Coraux, L. Marty, N. Bendiab, and J. Renard. Cathodoluminescence enhancement and quenching in type-I van der Waals heterostructures: Cleanliness of the interfaces and defect creation. *Phys. Rev. Materials*, 3:114001, 2019.
 - [20] S. Fiedler, S. Raza, R. Ai, J. Wang, K. Busch, N. Stenger, N. A. Mortensen, and C. Wolff. Importance of substrates for the visibility of “dark” plasmonic modes. *Opt. Express*, 28(9):13938–13948, 2020.
 - [21] D. Drouin, A. R. Couture, D. Joly, X. Tastet, V. Aimez, and R. Gauvin. CASINO v2.42—a fast and easy-to-use modeling tool for scanning electron microscopy and microanalysis users. *Scanning*, 29(3):92–101, 2007.



TOC Graphic